Geochemical Perspectives Letters

Modern mantle-like $\mu^{182}W$ signatures in Paleoarchean rocks from southern India

A. Ravindran, B.J. Peters, R. Yang, K. Mezger, J.J. Pakulla, F. Wombacher, M. Schönbächler, C. Münker

Supplementary Information

The Supplementary Information includes:

Geological Background

The Dharwar Craton (Fig. S-1), situated in the southern part of India, is divided into the older western and the younger eastern parts (Nath and Ramakrishnan, 1981), and has an association of greenstone belts, tonalite-trondhjemite-granite (TTG) suites and potassic granites (*e.g.*, Jayananda *et al.*, 2018) typical of Archean terranes. The western Dharwar Craton is further sub-divided into the older Sargur and younger Dharwar groups.

The bulk granitoid crust, composed of TTG suites, range in age from ~3.4 to 3.2 Ga and exposed in the Gorur-Holenarsipur region (*e.g.*, Jayananda *et al.*, 2015). Many other granitoid suites are exposed adjacent to greenstone belts (Fig. S-1).

The older Sargur Group, exposed mostly in the southern part of the craton, consists of komatiites, komatiitic basalts and tholeiitic rocks as linear greenstone belts that are associated with sedimentary rocks. Mafic and ultramafic rocks from this region yield whole rock errorchron ages of 3.35‑3.10 Ga (*e.g.*, Jayananda *et al.*, 2008; Maya *et al.*, 2017), which include the Holenarsipur, Ghattihosahalli and Banasandra greenstone belts (Fig. S-1; Table S-1). The younger Dharwar Group consists of the Bababudan (3.0‑2.9 Ga; Kumar *et al.*, 1996; Ravindran *et al.*, 2021), Chitradurga (~2.7 Ga; Jayananda, *et al.*, 2013), and Shimoga and Gadag greenstone belts (~2.6 Ga; Giri *et al.*, 2019; Sarma *et al.*, 2012) (Fig. S-1).

This study includes TTGs and granitic suites with known U-Pb zircon ages (Ravindran *et al.*, 2023) from this region and also from other areas that are associated with greenstone belts (Table S-1; Fig. S-1). Notably, most of the granitoids, especially TTGs, are coeval to the oldest mafic-ultramafic suites in the craton. A separate group of granitoids falling in the trondhjemite field, and having significantly high silica content and low alumina content (cf. Ravindran *et al.*, 2023), were also selected for this study. From their flat REE patterns and major element characteristics, these rocks are considered to be products of remelting, possibly at a shallow depth. Komatiitic and mafic rocks are from the Holenarsipur, Ghattihosahalli and Bababudan greenstone belts, and some from the Tarikere region that is recently distinguished for rocks of Sargur age (~3.25 Ga; Ravindran *et al.*, 2021).

Unaltered igneous and meta-igneous rock samples from different areas of the craton (Table S-1) of felsic, mafic and komatiitic compositions, ranging in ages from 3.4–3.0 Ga, were analyzed for their μ^{182}W values (12 samples and two replicates; Table 1; Tables S-2 and S-3) and trace element abundances (Table S-4). Additional isotope data on these samples is reported in Ravindran *et al.* (2021, 2023, 2024). A few samples with high W abundances, especially mafic and komatiitic rocks (Table S-4), were measured for their stable W ($\delta^{186/184}$W) isotope systematics (Table 1; Table S-5).

Methods

Preparation and data acquisition. The samples were crushed using an alumina-rich jaw crusher and powdered using an agate mill at the Institute of Geological Sciences, University of Bern, Switzerland. Aiming for a separation of 3-4 µg of W for μ^{182}W measurements, up to 2g of sample powders were digested in 60 ml Teflon beakers. The samples with 2g each were first digested using 20ml concentrated HF and 5 ml concentrated HNO_3 for two consecutive days. The same was repeated for komatiitic and Fe-rich tholeiitic rocks until the remaining solids were completely converted to fluorides. After drying, the samples were dissolved in ~20-25 ml concentrated HNO_3 overnight and dried. Then, 30 ml of concentrated HCl were added to each beaker and kept overnight on the hotplate at 120°C and dried down before 15-20 ml of 1M HCl were added to each beaker for loading 1g of the sample into the first cation columns. It was ensured that the amount of residual fluoride salts was kept to a minimum before samples were loaded onto the columns. Varying amounts of minimal residual salts from digestions of sample replicates (GHH 19.2, GHH 20.2 and sin 13) and in-house rock standards with different matrices did not show any μ^{182}W variations within uncertainties, and no stable W anomalies (μ^{183}W and μ^{184}W, Table S-2). This issue with residual salts was addressed in previous publications from the same lab (Tusch *et al.*, 2019, 2021, 2022; Pakulla *et al.*, 2025). The chemistry protocol used for radiogenic ^{182}W and stable W is given in Table S-6.

The analytical protocol for separation of W was followed according to Tusch *et al.* (2021, 2022) using a four-step chemical purification method, initially requiring a loading step comprising ~1g of sample material. Tungsten is separated along with HFSE from the first cation exchange resin (BioRad AG 50 W-X8 resin) after which separation from Ti is carried out using anion exchange resin (AG 1-X8 resin). The TEVA resin is used to separate W from Mo and Sn as a clean-up step, followed by purification of W using TODGA resin. The combined W cuts from each sample were further passed through TODGA and pre-filter resins as the final step to assure complete purification of the W cuts. Care was taken to prevent complete drying out of the W cuts from the same sample before combining them to avoid any possible fractionation. The separated W was repeatedly dried down with 80 µl 14M HNO_3-30% H_2O_2 mixtures at maximum 50 to 60°C to obtain high yields and prevent mass-independent effects on ^{183}W to a large extent (Tusch *et al.*, 2019). Replicate μ^{182}W measurements (Table S-2; Table 1) from separate rock digestions to ensure compositional homogeneity were done for two partially serpentinized komatiitic samples (GHH 19.2, GHH 20.2; Table S-2; Table 1; Fig. 1a) and also for an altered rhyolite from the Singhbhum Craton with different W yields (sin 13; Table S-3; Fig. 1a).

High-precision ^{182}W isotope measurements were done on a ThermoFisher© Neptune MC-ICPMS at the University of Cologne, Germany and sample solutions were introduced using a Cetac Aridus II desolvator. Each measurement day was started with gain amplifications and baseline determination for 1200s. Samples were bracketed using a NIST SRM 3163 standard solution that was matched in concentration with that of the respective sample and measured at ^{182}W ion beam intensities of =~15-20V. An additional on-peak-zero subtraction from the background solution (0.56M HNO_3-0.24M HF) for each measurement was carried out, and are reported (Tables S-2 and S-3), and the results also compared with non-on-peak-zero-corrected values. Results are reported in µ-notation relative to the NIST standard solution. All samples were repeatedly analyzed (n=7 to 24) and the uncertainties for their average μ^{182}W values are reported at 95% confidence interval assuming 5% scatter (Tables S-2 and S-3). Throughout individual measurements, the W isotope ratios and standard errors were monitored. Mass bias correction was done using the exponential mass fractionation law and both, $^{186}W/^{184}W$=0.92767 and $^{186}W/^{183}W$=1.9859. The reliability and consistency of ^{182}W isotope separation and measurements of the samples in each session are tested by repeated measurements of in-house rock standards AGC 351 and 160245 (Fig. 1a in the main manuscript), representing a TTG from the Ancient Gneiss Complex and a komatiite from the Ruth Well Formation in western Australia. Both have $\mu^{182}W$ values in agreement to previously published data from the same laboratory (Fig. 1a; Table S-3; Tusch *et al*., 2022; Pakulla *et al*., 2025). The long-term average 95% CI of AGC 351 is shown in Fig.1. The $\mu^{182}W$ values were indistinguishable from that of previous measurements (Tusch *et al*., 2022; Table S-3). To evaluate potential heterogeneities of sample powders, samples with high W/Th as a result of surrounding W mineralization (W/Th=1572; samples GHH 19.2, GHH 20.2; Table S-1) were digested twice each and measured, consisting of 12 and 24 individual measurement sets (Table S-2) to identify small $\mu^{182}W$ anomalies if present. Tests for $^{182}W/^{184}W$ fractionation as a result of low yields were also carried out on an altered rhyolite sample from the Singhbhum Craton (sample sin 13; Table S-2), and this study finds that the $\mu^{182}W$ values are indistinguishable from the standard solution at 47% and 98% W yield (Fig. 1a in the main manuscript). No evidences for mass-dependent fractionation of stable W isotopes were observed as they show no resolvable anomalies from 0 (Tables S-2 and S-3).

The stable W isotope systematics of mafic and komatiitc rock samples taken for this study were acquired by employing the double spike (^{180}W-^{183}W) technique established at the University of Cologne, Germany (Kurzweil *et al.*, 2018). This was to precisely correct for mass-dependent W isotope fractionation during sample processing and instrumental measurement. A three-step column chemistry (Kurzweil *et al.*, 2018) was carried out for the samples to remove isobaric interferences of Hf and Ta. Apart from the additional cleaning procedures using TODGA and pre-filter resins, the protocol for stable W separation was the same as that used for radiogenic ^{182}W. Rigorous digestions procedures were repeated to avoid residual fluoride precipitation. The separation procedure for W involved a BioRad AG 50 W-X8 cation exchange resin (15 mL), followed by an anion resin AG 1 X8 (2 mL), where W is collected with 3 M HNO_3- 0.2 M HF. The final chemistry with 1 mL Eichrom TEVA resin was used to separate W from elements such as Ti, Zr, Hf and Mo. The reference material OU-6 yielded a value of +0.115±0.018‰ (external 2SD; Table S-5) and is consistent with previously published results (Yang *et al.*, 2025). The $\delta^{186/184}W$ values of selected samples range from -0.088±0.018‰ to +0.264±0.018‰ (Table 1; Table S-5). Uncertainties refer to the external 2SD of rock standard OU6-1 measured along with the samples (Supplementary Information; Kurzweil *et al.*, 2020; Yang *et al.*, 2025). The average yield of all samples is over 60% (Table S-5). Pure W reference solution Alfa Aesar was measured in each measurement sequence.

High-precision ^{142}Nd isotope measurements were done on a Thermo Scientific Triton TIMS at ETH Zurich, Switzerland. The sample preparation and analytical protocol are as reported in Ravindran *et al*. (2024). The measured $\mu^{142}Nd$ and $\varepsilon^{143}Nd_i$ values of the samples are plotted in Figure 3 in the main manuscript. Additionally, the Nd isotope compositions of highly silicic trondhjemites from the Dharwar Craton that were not studied previously are also plotted. The external 2SD of JNdi standards from four sessions (after cup change) is shown in Fig.3c.

Trace element and some of the major element abundances were measured on a ThermoFisher® iCAP Quadrupole ICP-MS at the University of Cologne (Table S-4). Internal standard elements (Rh and Re) were added to about 50 mg sample powder and the weight of the sample and internal standard was precisely recorded for later quantification (cf. Braukmüller *et al*., 2018; Pakulla *et al*., 2023). Samples were digested in 3 mL concentrated HNO_3 and HF (1:1) in Parr pressure digestion vessels at 180 °C for 48 hours. After the solutions were dried down to incipient dryness, 5 ml of concentrated HNO_3 were added and the solutions dried down again. The nitric acid dry-down step, which serves to remove insoluble fluorides, was repeated twice. Following complete dry-down, the samples were redissolved in 2.8 N HNO_3 and diluted in two steps to finally yield a 4000-fold dilution in 0.28 N HNO_3.

Measurements were carried out in two sessions in 2023 and 2024. External calibration utilized solutions prepared from the reference materials BIR-1, BHVO-2, BCR-2, JB-2, AGV-2 and in 2024 also BE-N using preferred values from GeoREM (Jochum *et al.*, 2005) complemented by isotope dilution data from Kirchenbaur *et al.* (2018), Kurzweil *et al.* (2018), Braukmüller *et al.* (2020). In 2023, each sample was analysed twice and basalt BVA-1 from the GeoPT proficiency testing (Webb *et al.*, 2021) was prepared and analysed together with the samples for quality control. In 2024, each sample was analysed four times and the OKUM komatiite reference material was prepared and analysed along with the samples. Most data agree with the reference values to within 10%, but seven datapoints deviate by up to 19% (Table S-4). The trace element data presented in this study is also compared with previously reported measurements (Table S-4; Ravindran *et al*., 2023).

Robustness of acquired μ¹⁸²W values. Instrumental mass bias correction was done relative to two W isotope ratios ($^{186}W/^{184}W$=0.92767 and $^{186}W/^{183}W$=1.9859) using the exponential law, of which the $^{186}W/^{184}W$ normalized value is given more importance due to the mass-independent effects on ^{183}W, which can create bias by analytical artefacts as a result of odd-even isotope ratio effects (Cook and Schönbächler, 2016). Still, both μ-values are compared and evaluated to understand the efficiency of nuclear field shift correction shown as a reference line (Fig. S-2), and the inclusion or omission of individual ^{182}W measurements were based on rigorous data reduction (Tables S-2 and S-3).

Trace Element Abundances

The felsic, mafic and komatiitic rocks that were taken for this study were measured for their trace element abundances, which were also compared with previous measurements of the same samples (Ravindran *et al.*, 2021, 2023).

The mafic rocks show a slight LREE enrichment when compared to the HREE (Fig. S-3). The komatiite and komatiitic basalt from the Holenarsipur greenstone belt (SG24.1, SG24.3) have relatively flat REE patterns (Fig. S-3). Among the two komatiitic basalts showing slight positive Eu anomaly (BB8.3 and GHH 20.2), the sample GHH20.2 shows a significant LREE depletion (Fig. S-3).

All felsic rocks show significant Ti depletion. Among these, the TTGs and granites (granitic gneisses) show significant HREE depletion over LREE and a notable Nb-Ta depletion (Fig. S-3). The high silica-rich, low alumina, trondhjemites have LREE abundances similar to that of the TTGs and granites, but show prominent HREE enrichment. They also show enrichment of Nb and Ta compared to the other granitoids (Fig. S-3).

Effects of Secondary W

Precambrian rocks were commonly subject to post-emplacement mineralogical and chemical modification, and samples from the Dharwar Craton taken for this study may likewise have been modified by late addition of W. Such secondary W (Fig. 2 in the main manuscript) could have infiltrated these open magmatic systems from neighboring country rocks or other sources at a certain period of time, and become incorporated into mineral phases such as serpentine, Ti-rich minerals, phlogopite, and sulfides or could have been trapped along grain boundaries (e.g., Liu *et al*., 2018). Hence, such secondary processes may have also modified the primary Hadean $\mu^{182}W$ as has been suggested for the Singhbhum Craton (cf. Messling *et al*., 2023) and other Archean suites (*e.g.*, SW Greenland, Rizo *et al*., 2016; Kurzweil *et al*., 2020).

The rock samples from Dharwar Craton taken for this study were rigorously tested for the effects of W abundances, that were derived as a result of secondary processes, on their $\mu^{182}W$ signatures (see the Discussion in the main manuscript). This can be tested by the relationship between W/Th and Th, as Th is less mobile during secondary processes such as alteration hydrothermalism or metasomatism (e.g., Münker *et al*., 2004). Globally, significantly large $\mu^{182}W$ anomalies are reported predominantly in mafic to komatiitic rocks, often with variable W/Th ratios (Fig. 1b in the main manuscript). The felsic samples and one komatiitic sample from the Dharwar craton have mantle-like W/Th ratios (0.02-0.24; König *et al*., 2011; Table 1), whereas the others display higher W/Th, suggesting that they accumulated W after emplacement. This komatiitic sample that has a canonical W/Th ratio (SG 24.3) is not spatially far from another komatiite (SG 24.1; Table S-1) that has a non-canonical W/Th. This could imply that the secondary W has a local source. For the test, two samples were collected from an area that is reported to host abundant scheelite veins in mafic-ultramafic rocks (Ghattihosahalli greenstone belt; Srinivasaiah *et al*., 2015). The grade of mineralization and the exact source of W is under-studied. These rocks are also identified to be rich in Ba, and the overlying sedimentary rocks are rich in Cr (fuchsite-rich quartzite), Ba (barite) and B (tourmaline grains) (Ravindran *et al*., 2020). These observations indicate local hydrothermalism (Srinivasaiah *et al.*, 2015) or metasomatism with the fluids originating from the surrounding rocks and possibly seawater (Ravindran *et al.*, 2020). The source composition is beyond the scope of this study, but some clues were obtained from elemental and W isotope tests (Fig. S-4, Fig. 2). Only one of these rocks were measured for trace elements (Table S-4), with the field observation that both rocks come from the same protolith (Ravindran *et al.*, 2021). Nevertheless, these two samples were measured repeatedly ('n'), both according to our laboratory protocol (n=13) and also for a longer run duration (n=24) (Table S-3) to obtain precise μ^{182}W values by possible additions of secondary W. These samples do not show any resolvable μ^{182}W anomalies, similar to that of rocks having canonical and non-canonical W/Th.

Our data indicates no correlation between the measured μ^{182}W values and the measured concentrations of W and W/Th ratios of the samples (Fig. 2a and b). As an additional proxy, stable W isotope data were used from rocks that show a non-canonical W/Th, especially mafic and komatiitic rocks. No correlation was found between $\delta^{186/184}$W and μ^{182}W (Fig. 2c), and W/Th (Fig. 2d). Ratios of W/Th and W/U form a trend, which is a sign of magmatic differentiation (Fig. S-4a; e.g., Liu *et al.*, 2018; Mei *et al.*, 2020). However, the mobility of W through aqueous fluids could lead to redistribution of W in the original protoliths (e.g., König *et al*., 2011). Another proxy that is incompatible in igneous reservoirs is Nb/Th, and most of the samples define a trend with W/Th (Fig. S-4b). The only exceptions are the W-mineralized sample and two TTGs that have a rutile-rich protolith identified from their trace element signatures. These two incompatible tracers (W/U and Nb/Th) show no trend with μ^{182}W values of the samples (Fig. S-4c, e), indicating that these are not connected by magmatic differentiation either. However, the $\delta^{186/184}$W values of some of the mafic and ultramafic rocks indicate a partial trend (Fig. S-4d, f), and they do not correlate with W/Th (Fig. 2d). This could possibly be related to similar oxidation states or D-values of W and U.

It can be added that the absence of a correlation between $\delta^{186/184}$W of mafic and komatiitic samples in the craton and their μ^{182}W values likely reflects their derivation from two distinct processes- Hadean magmatic and later local metasomatic processes. The $\delta^{186/184}$W values poorly correlate with some of the incompatible elements, but this needs to be studied further based on local processes affecting these signatures, which is beyond the scope of this study. Contribution of W from neighbouring granitoids (e.g., Messling *et al.*, 2023) to the mafic and komatiitic rocks may also be considered. However, this study confirms that the μ^{182}W values of all samples (felsic, mafic and komatiitic) do not correlate with any of the tracers showing no evidence for being affected by metasomatism, hydrothermal alteration or magmatic differentiation despite their age of emplacement.

The μ^{182}W values of Precambrian rocks from around the world are mostly positive (Fig. 1b in the main manuscript) despite their variable and non-canonical W/Th ratios. Therefore, the mobility of W in the mafic and komatiitic rocks does not lead to homogenisation of μ^{182}W values of rocks that were spatially and temporally distributed in the Dharwar Craton. If homogenisation occurred by magmatic processes, some correlation is to be expected between μ^{182}W and $\delta^{186/184}$W values of the samples (Fig. 2c), which is, however, not observed.

Hadean Mantle Heterogeneities

Mantle heterogeneities in the Hadean can be understood using a variety of isotope systematics, the most sensitive being short-lived isotope systems such as the ^{182}Hf-^{182}W and the ^{146}Sm-^{142}Nd. Combined isotope studies on rocks from different parts of the world are limited due to limited exposure of rocks and the necessity of measurements at high precision. From available data that are largely based on rocks from Greenland and Canada (Fig. 1b and Fig. 3c in the main manuscript), it can be observed that μ^{142}Nd anomalies tend to disappear with time, which is also observed in the case of the rocks from the Dharwar Craton (Fig. 3). However, μ^{182}W values of Precambrian rocks from around the world do not show this trend and show predominantly excesses compared to the modern mantle (μ^{182}W average= +12.7±1.2; Tusch *et al.*, 2021), with only one exception (Kaapvaal Craton; Tusch *et al.*, 2022; Puchtel *et al.*, 2016a) that gives evidence for μ^{182}W and μ^{142}Nd deficits. Rocks from the Canadian Shield predominantly show μ^{182}W excesses and μ^{142}Nd deficits (e.g., O'Neil *et al.*, 2008; Reimink *et al.*, 2018), which could be due to silicate differentiation recorded at ~4.4 Ga (e.g., Morino *et al.*, 2017; Caro et al., 2017). Rocks from the North Atlantic Craton shows μ^{182}W and μ^{142}Nd excesses (O'Neil *et al*., 2016; Rizo *et al*., 2013), which is suggested to be due to a missing late veneer component (Tusch *et al*., 2019) and a silicate differentiation age of ~4.4 Ga (Saji *et al*., 2018; Hasenstab-Dübeler *et al*., 2022). Earlier studies (e.g., Rizo *et al*., 2013) had suggested that different mechanisms of origin were involved in the decoupling of the $\mu^{182}W$ and $\mu^{142}Nd$ values in these rocks. The Pilbara and Saõ Francisco cratons, on the other hand, show $\mu^{182}W$ excesses and no $\mu^{142}Nd$ anomalies (Murphy *et al*., 2021; Tusch *et al*., 2021; Leitzke *et al*., 2024). Rocks from the Kaapvaal Craton could have undergone an addition of a Hadean protocrust that had formed right after magma ocean solidification (Tusch *et al*., 2022), or crystal-liquid fractionation in an early magma ocean (Puchtel *et al.*, 2016a). Eoarchean rocks from the Anshan Complex show $\mu^{182}W$ excesses (Mei *et al*., 2020), which is proposed to be due to early Hadean (>4.5 Ga) silicate differentiation. Meso- and Neoarchean rocks from the Baltic and Fennoscandian Shields show $\mu^{182}W$ excesses (Touboul *et al*., 2012; Puchtel *et al*., 2016b). The Indian cratons show small $\mu^{142}Nd$ anomalies indicating silicate differentiation ages at ~4.2-4.15 Ga (Maltese *et al*., 2022; Ravindran *et al*., 2024), with another older differentiation event at ~4.38 Ga (Ravindran *et al*., 2024). The first $\mu^{182}W$ data recorded from an Indian craton shows no anomalies, and resemble the Bulk Silicate Earth or the modern mantle (this study). Apart from this, the rocks from the Dharwar Craton show $\mu^{182}W$ values indistinguishable from the modern mantle whereas coeval rocks from the Pilbara, North Atlantic and Kaapvaal Cratons, and Baltic, Fennoscandian Shields exhibit anomalous $\mu^{182}W$.

A lack of strict correlation of Hf-W and Sm-Nd short-lived systems in the rocks from the Dharwar Craton implies decoupling at some point in early Earth history. Lack of $\mu^{182}W$ anomalies in these rocks could imply that they achieved the full late veneer inventory before their emplacement age. Core-mantle interaction is also not observed in these rocks, even in deeper mantle rocks such as komatiites. Different mechanisms responsible for the evolution and retention of these isotope systems is not observed in the $\mu^{182}W$ values of these rocks, as they have a consistently non-anomalous $\mu^{182}W$ value for different rock types ranging in age from 3.4 to 3.0 Ga. Influence of multiple Hadean source reservoirs in the lower mantle that could modify the original $\mu^{182}W$ values, which was suggested for rocks from the nearby Deccan Traps (Pakulla *et al*., 2025), is also not visibly found in the $\mu^{182}W$ signatures of rocks from the Dharwar Craton. A silicate differentiation event after early Hadean (<4.5 Ga) or the dilution of anomalous $\mu^{182}W$ before ~4.38 Ga (see Discussion in the main manuscript). Nevertheless, this $\mu^{182}W$ signatures of rocks from the Dharwar Craton, by itself, is an important evidence for mantle heterogeneity and further postulate that not all mantle reservoirs followed a uniform evolutionary trajectory following core formation.

Supplementary Tables

Table S-1 Sample information of felsic, mafic and komatiitic rocks from the Dharwar Craton used for this study.

Sample name	Rock type	Region	Location
GHH 22.1	Granitic gneiss	Janakal; near Ghattihosahalli greenstone belt	13°54'26.90"N 76°19'06.70"E
GHH 22.3	Granitic gneiss	Janakal; near Ghattihosahalli greenstone belt	13°54'26.90"N 76°19'06.70"E
GHH 22.4	Tonalite	Janakal; near Ghattihosahalli greenstone belt	13°54'26.90"N 76°19'06.70"E
SG 29.1	Trondhjemite	Gorur; close to Holenarsipur greenstone belt	12°45'49.60"N 76°09'12.60"E
SG 32.1	Granitic gneiss	Gorur; close to Holenarsipur greenstone belt	12°49'56.00"N 76°04'16.90"E
SG 32.2	Trondhjemite	Gorur; close to Holenarsipur greenstone belt	12°49'56.00"N 76°04'16.90"E
SG 34.1	Tonalite	Gorur; close to Holenarsipur greenstone belt	12°54'31.30"N 76°09'11.30"E
HNL 6.3	Trondhjemite	Honnali; near Shimoga greenstone belt	14°11'18.80"N 75°36'12.70"E
CHK 36.1	Granitic gneiss	Chikmagalur; close to Bababudan greenstone belt	13°16'24.50"N 75°49'45.30"E
SG 30.2	Low-Al high silica trondhjemite	Gorur; close to Holenarsipur greenstone belt	12°54'06.30"N 76°04'59.70"E
SG 30.3	Low-Al high silica trondhjemite	Gorur; close to Holenarsipur greenstone belt	12°54'06.30"N 76°04'59.70"E
CHK 38.1	Low-Al high silica trondhjemite	Chikmagalur; close to Bababudan greenstone belt	13°16'05.60"N 75°53'09.70"E
SG 24.1	komatiite	Holenarsipur greenstone belt	12°50'18.00"N, 76°12'13.70"E
SG 24.3	komatiitic basalt	Holenarsipur greenstone belt	12°50'38.90"N, 76°12'10.00"E
GHH 20.2	komatiitic basalt	Ghattihosahalli greenstone belt	13°59'41.60"N, 76°16'52.10"E
GHH 19.2	komatiitic basalt	Ghattihosahalli greenstone belt	13°59'16.00"N, 76°17'13.20"E
BB 8.3	komatiitic basalt	near Tarikere; represents Sargur Group	13°41'37.30"N, 75°49'52.80"E
BB 8.4	andesite	near Tarikere; represents Sargur Group	13°41'37.30"N, 75°49'52.80"E
BB 8.5	basaltic andesite	near Tarikere; represents Sargur Group	13°41'53.40"N, 75°50'02.00"E
BB 37.5	komatiitic basalt	Bababudan greenstone belt	13°27'02.70"N, 75°48'04.60"E
GHH 21.1	basalt	Ghattihosahalli greenstone belt	13°58'55.80"N, 76°16'02.40"E

Table S-2 A summary of final values of ^{182}W isotope measurements of samples from the Dharwar Craton. One sample HNL 6.3 shows stable W anomalies, which could be related to nuclear field effects of the odd isotope ^{183}W. The full version of Table S-2 (.xlsx) is available for download from the online version of this article at https://doi.org/10.7185/geochemlet.2616.

Sample	Final values after data reduction							
	Normalization to $^{186}W/^{184}W$ = 0.92767				Normalization to $^{186}W/^{183}W$ = 1.9859			
	$\mu^{182}W_{meas}$	± 95% CI	$\mu^{183}W_{meas}$	± 95% CI	$\mu^{184}W_{meas}$	± 95% CI	$\mu^{182}W_{corr}$	± 95% CI
GHH 19.2	1.4	3.0	-0.1	2.0	0.1	1.3	1.2	2.8
GHH 19.2	-0.6	2.1	-1.2	1.3	0.8	0.9	-1.7	2.0
GHH 20.2	-0.4	2.5	0.9	2.3	-0.6	1.5	-0.6	2.9
GHH 20.2	-1.1	1.7	0.3	1.5	-0.2	1.0	-1.1	1.9
SG 24.1	0.5	2.5	-2.6	1.9	1.7	1.2	1.8	2.6
BB 8.3	-3.3	3.3	2.8	6.5	-1.9	4.3	-4.2	6.0
BB 8.5	-0.4	2.1	-0.8	1.7	0.5	1.1	-2.1	2.1
SG 30.3	1.2	3.2	-0.5	4.1	0.3	2.7	0.9	3.9
HNL 6.1	1.9	3.6	0.8	3.2	-0.5	2.1	-0.6	4.0
SG 34.1	1.6	2.2	-0.1	3.5	0.0	2.4	-1.0	2.6
HNL 6.3	-2.6	3.2	-3.9	2.6	2.6	1.7	-5.5	2.9
SG 32.2	-1.7	3.1	0.7	6.0	-0.5	4.0	-3.8	4.1
GHH 22.4	-1.8	1.9	1.6	1.8	-1.1	1.2	-2.5	2.3
SG 24.3	3.0	4.1	-2.4	2.2	1.6	1.5	2.2	3.7
Yield tests								
Sin 13	1.1	3.3	-0.2	2.1	0.1	1.4	2.7	2.7
Sin 13	2.0	2.7	-0.3	2.3	0.2	1.6	2.2	2.9

Table S-3 A summary of final values of ^{182}W isotope measurements of in-house rock standards. The full version of Table S-3 (.xlsx) is available for download from the online version of this article at https://doi.org/10.7185/geochemlet.2616.

Sample	Final values after data reduction							
	Normalization to $^{186}W/^{184}W$ = 0.92767				Normalization to $^{186}W/^{183}W$ = 1.9859			
	$\mu^{182}W_{meas}$	± 95% CI	$\mu^{183}W_{meas}$	± 95% CI	$\mu^{184}W_{meas}$	± 95% CI	$\mu^{182}W_{corr}$	± 95% CI
AGC 351	-0.2	2.1	-0.3	2.4	0.2	1.6	-0.5	1.9
AGC 351	-2.2	3.0	1.0	1.5	-0.9	1.0	-1.7	2.8
AGC 351	-1.7	3.0	-0.1	1.4	0.1	0.9	-2.5	2.7
AGC 351	-0.7	2.1	0.5	2.0	-0.4	1.3	0.2	1.9
AGC 351	2.1	2.5	1.5	1.8	-1.0	1.2	2.5	2.6
160245	7.8	1.8	-3.7	2.1	2.5	1.4	7.4	1.5
160245	6.4	3.0	-0.9	2.8	0.6	1.9	7.5	2.5
160245	7.6	2.7	-1.3	3.2	0.9	2.1	8.0	1.8
160245	5.9	2.6	-3.5	1.9	2.3	1.3	6.2	2.9

Table S-4 Trace element and selected major element abundances of samples from the Dharwar Craton taken for this study. Relative deviation (%) from previously published data (Ravindran *et al*., 2021, 2023) is also provided.

Table S-4 (.xlsx) is available for download from the online version of this article at https://doi.org/10.7185/geochemlet.2616.

Table S-5 Stable W isotope ($\delta^{186/184}$W) data of samples taken for this study

Sample	$\delta^{186/184}$W (‰)	Internal 2 SE (‰)	W concentration given by double spike dilution (ppm)	Yield (%)
OU-6	+0.115	0.009	1.102	43
BB 8.3	-0.088	0.011	0.231	39
BB 8.5	+0.187	0.010	0.291	55
GHH 20.2	+0.264	0.009	111.634	70
SG 24.3	+0.120	0.012	0.174	42
SG 24.1	+0.175	0.008	0.635	78
Blank	85.9 pg			

Table S-6 The W-separation protocol used for this study.

Step	Acid volume (ml)	Reagent
Column 1- 15 ml BioRad AG 50W-X8 resin in BioRad Econo-Pac columns; reservoir- 18 ml		
Pre-cleaning	2 column reservoirs	6 M HCl
Equilibrate	2 column reservoirs	1 M HCl- 1 Vol% H_2O_2
Load, collect HFSE	Up to 20 ml	1 M HCl- 1 Vol% H_2O_2
Collect HFSE	3 ml × 5	1 M HCl- 1 Vol% H_2O_2
Elute major elements	40 ml × 2	1.8 M HCl
Elute MREE-HREE & Sr	30 ml × 2	6 M HCl
Elute remaining LREE & Ba	40 ml	6 M HCl
Rinse matrix	2 column reservoirs	6 M HCl
Elute Th	1 column reservoir	2 M HF
Rinse remaining matrix	1 column reservoir	6 M HCl
Rinse remaining matrix	2 column reservoirs	1 M HCl

Table S-6 continued.

Step	Acid volume (ml)	Reagent
Column 2- 2 ml BioRad AG 1-X8 resin in BioRad Poly-Prep columns; reservoir- 10 ml		
Equilibrate	2 column reservoirs	1 M HCl- 1 Vol% H_2O_2
Load, elute Ti-Zr-Hf	35 ml	1 M HCl- 1 Vol% H_2O_2
Elute Ti-Zr-Hf & Nb	3 ml × 5	1 M HCl- 1 Vol% H_2O_2
Rinse	3 column reservoirs	2 M HF
Collect W & Mo	3 ml × 5	3 M HNO_3 (3 M HNO_3- 0.2 M HF for stable W chemistry)
Rinse	1 column reservoir	3 M HNO_3- 0.2 M HF-1 Vol% H_2O_2
Rinse	1 column reservoir	0.56 M HNO_3- 0.24 M HF
Rinse	2 column reservoirs	3 M HNO_3- 0.2 M HF
Rinse	1 column reservoir	6 M HCl
Rinse	1 column reservoir	1 M HCl
Column 3- 1 ml Eichrom TEVA resin in Spectra/Chrom 45 µm PP mini-columns ; reservoir- 7 ml		
Equilibrate	2 column reservoirs	6 M HCl
Load, elute remaining Ti-Zr-Hf	1 ml	6 M HCl
Elute Ti-Zr-Hf	2 ml × 1 1 ml × 3	6 M HCl
Collect W	3 ml × 3-4	4 M HCl
Elute Mo	3 ml × 3	3 M HNO_3
Rinse	2 column reservoirs	3 M HNO_3- 0.2 M HF
Rinse	2 column reservoirs	3 M HNO_3
Rinse	1/2 column reservoir	2 M HF
Rinse	1 column reservoir	6 M HCl
Rinse	1 column reservoir	1 M HCl
W clean up (only for ^{182}W) - 1 ml TODGA resin in Spectra/Chrom 45 µm PP mini-columns ; reservoir- 6.5 ml		
Pre-cleaning	1 column reservoir	0.56 M HNO_3- 0.24 M HF
Equilibrate	2 column reservoirs	6 M HCl
Load	9-12 ml	4 M HCl
Rinse	4 column reservoirs	3 M HNO_3
Collect W	3 ml × 4-5	0.56 M HNO_3- 0.24 M HF
Rinse	1 column reservoir	0.56 M HNO_3- 0.24 M HF
Rinse	1 column reservoir	3 M HNO_3- 0.2 M HF
Rinse	1 column reservoir	2 M HF
Rinse	1 column reservoir	1 M HCl

Supplementary Figures

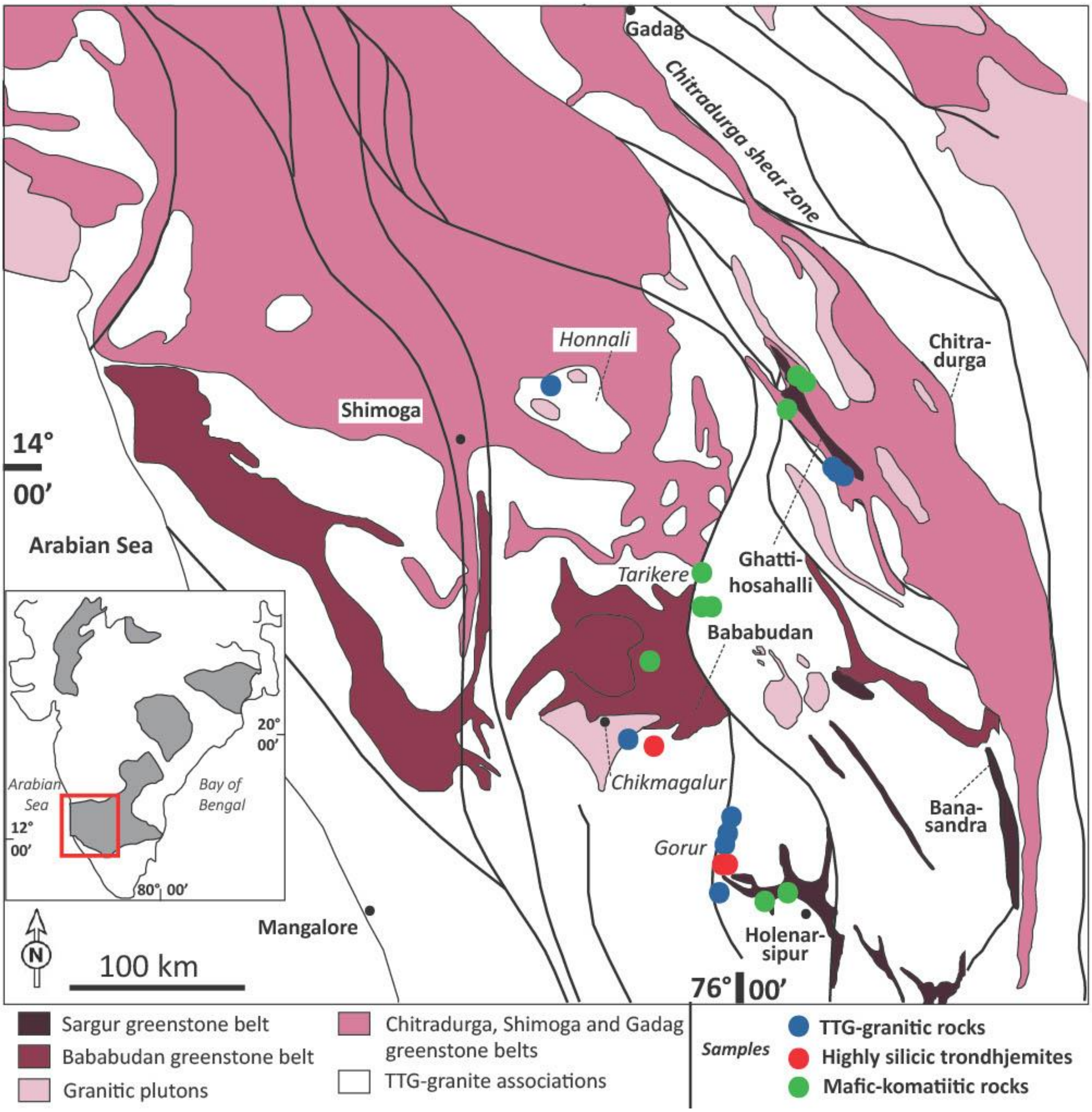

Figure S-1 A simplified geological map of the western Dharwar Craton, as modified from Ravindran *et al.* (2024) and Jayananda *et al.* (2018). The sub-figure shows the location of the Dharwar Craton along with the other four Archean cratons in the Indian subcontinent. Approximate locations used for sample collection are shown and the exact locations given in Table S-1.

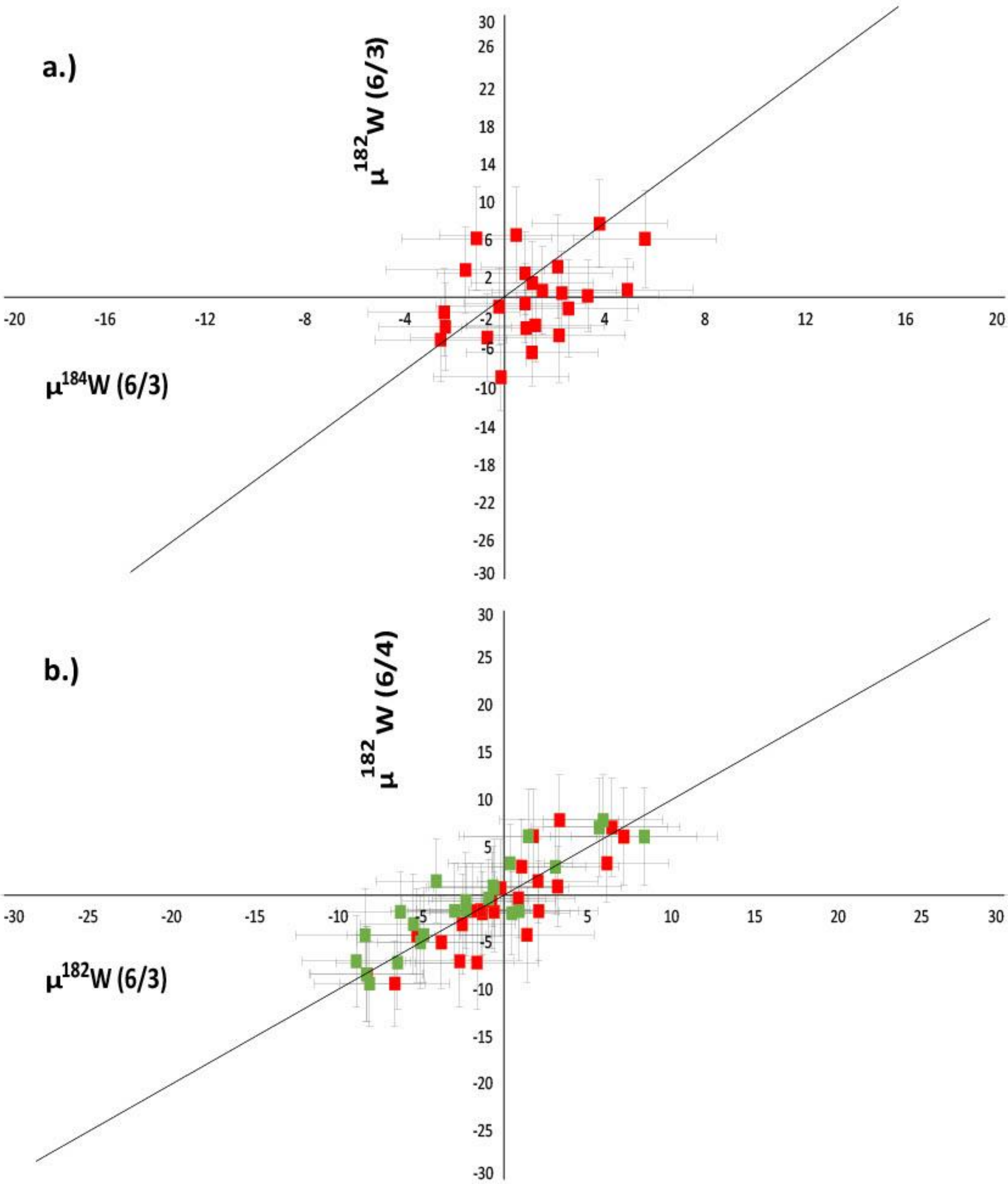

Figure S-2 Mass-bias corrected W isotope ratios of sample GHH 19.2 **(a)** μ^{182}W (6/3) vs μ^{184}W (6/3) before internal corrections for nuclear field shift on μ^{182}W (6/3) **(b)** μ^{182}W (6/4) vs μ^{182}W (6/3) before (red squares) and after (green squares) nuclear field shift correction (Cook and Schönbächler, 2016). The reference line for nuclear field effects is shown in both **(a)** and **(b)**.

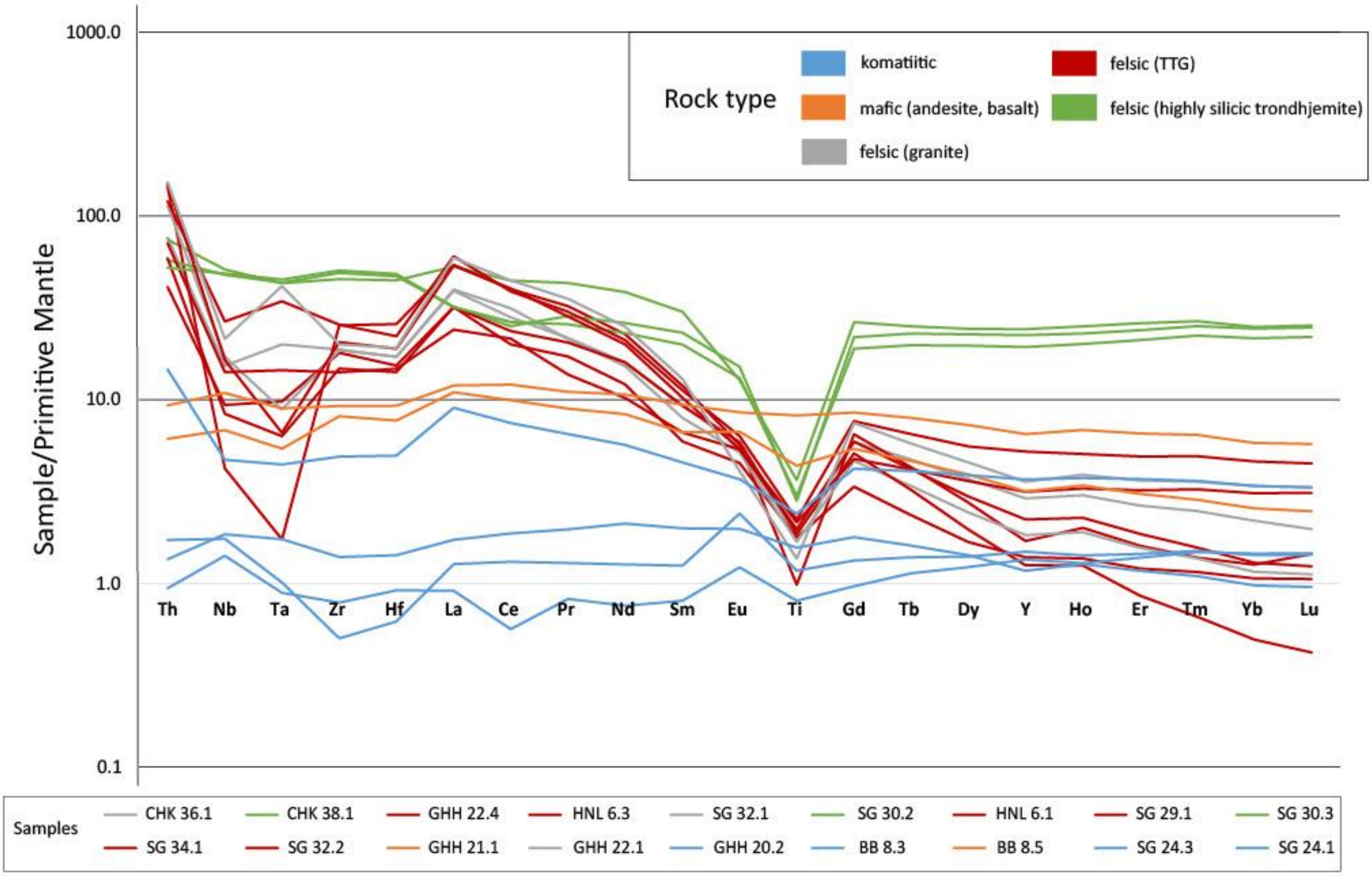

Figure S-3 Spidergram of rock samples taken for this study. The values are also compared with the values reported in Ravindran *et al.* (2023).

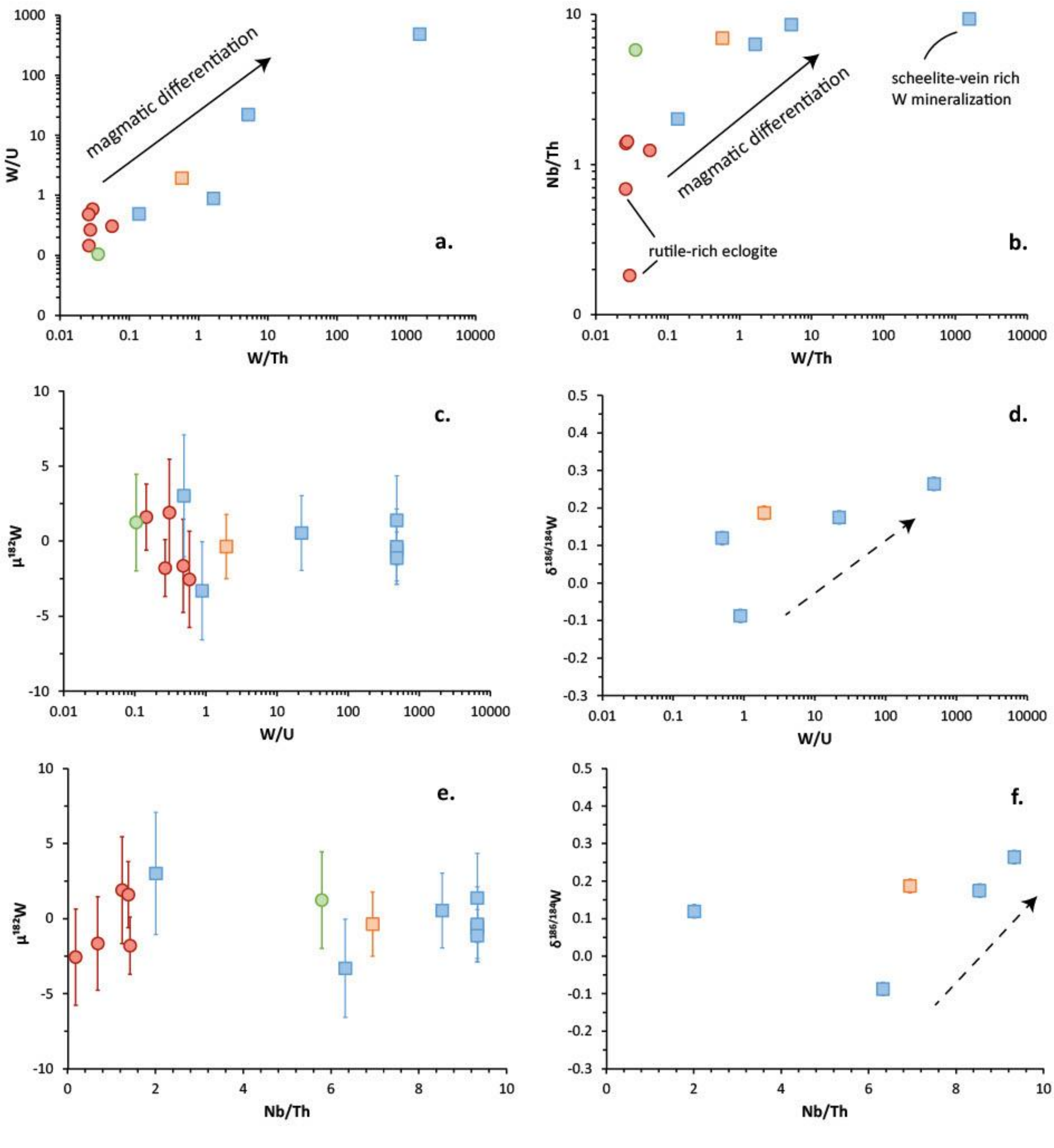

Figure S-4 Proxies of incompatible elements against W isotopes **(a)** W/U vs. W/Th **(b)** Nb/Th vs. W/Th **(c)** μ^{182}W vs. W/U **(d)** $\delta^{186/184}$W vs. W/U **(e)** μ^{182}W vs. Nb/Th **(f)** $\delta^{186/184}$W vs. Nb/Th.

Supplementary Information References

Braukmüller, N., Wombacher, F., Hezel, D.C., Escoube, R., Münker, C. (2018) The chemical composition of carbonaceous chondrites: Implications for volatile element depletion, complementarity and alteration. *Geochimica et Cosmochimica Acta* 239, 17–48. https://doi.org/10.1016/j.gca.2018.07.023

Braukmüller, N., Wombacher, F., Bragagni, A., Münker, C. (2020) Determination of Cu, Zn, Ga, Ag, Cd, In, Sn and Tl in Geological Reference Materials and Chondrites by Isotope Dilution ICP-MS. *Geostandards and Geoanalytical Research* 44, 733–752. https://doi.org/10.1111/ggr.12352

Caro, G., Morino, P., Mojzsis, S.J., Cates, N.L., Bleeker, W. (2017) Sluggish Hadean geodynamics: Evidence from coupled ^{146,147}Sm–^{142,143}Nd systematics in Eoarchean supracrustal rocks of the Inukjuak domain (Québec). *Earth and Planetary Science Letters* 457, 23–37. https://doi.org/10.1016/j.epsl.2016.09.051

Cook, D.L., Schönbächler, M. (2016) High-precision measurement of W isotopes in Fe–Ni alloy and the effects from the nuclear field shift. *Journal of Analytical Atomic Spectrometry* 31, 1400–1405. https://doi.org/10.1039/C6JA00015K

Giri, A., Anand, R., Balakrishnan, S., Dash, J.K., Srinivasa Sarma, D. (2019) Neoarchean magmatism in Shimoga greenstone belt, India: Evidence for subduction-accretion processes in the evolution of the western Dharwar stratigraphy. *Lithos* 330–331, 177–193. https://doi.org/10.1016/j.lithos.2019.02.015

Hasenstab-Dübeler, E., Tusch, J., Hoffmann, J.E., Fischer-Gödde, M., Szilas, K., Münker, C. (2022) Temporal evolution of ^{142}Nd signatures in SW Greenland from high precision MC-ICP-MS measurements. *Chemical Geology* 614, 121141. https://doi.org/10.1016/j.chemgeo.2022.121141

Jayananda, M., Kano, T., Peucat, J.-J., Channabasappa, S. (2008) 3.35 Ga komatiite volcanism in the western Dharwar craton, southern India: Constraints from Nd isotopes and whole-rock geochemistry. *Precambrian Research* 162, 160–179. https://doi.org/10.1016/j.precamres.2007.07.010

Jayananda, M., Peucat, J.-J., Chardon, D., Krishna Rao, B., Fanning, C.M., Corfu, F. (2013) Neoarchean greenstone volcanism and continental growth, Dharwar craton, southern India: Constraints from SIMS U–Pb zircon geochronology and Nd isotopes. *Precambrian Research* 227, 55–76. https://doi.org/10.1016/j.precamres.2012.05.002

Jayananda, M., Chardon, D., Peucat, J.-J., Fanning, C.M. (2015) Paleo- to Mesoarchean TTG accretion and continental growth in the western Dharwar craton, Southern India : Constraints from SHRIMP U–Pb zircon geochronology, whole-rock geochemistry and Nd–Sr isotopes. *Precambrian Research* 268, 295–322. https://doi.org/10.1016/j.precamres.2015.07.015

Jayananda, M., Santosh, M., Aadhiseshan, K.R. (2018) Formation of Archean (3600–2500 Ma) continental crust in the Dharwar Craton, southern India. *Earth-Science Reviews* 181, 12–42. https://doi.org/10.1016/j.earscirev.2018.03.013

Jochum, K.P., Nohl, U., Herwig, K., Lammel, E., Stoll, B., Hofmann, A.W. (2005) GeoReM: A New Geochemical Database for Reference Materials and Isotopic Standards. *Geostandards and Geoanalytical Research* 29, 333–338. https://doi.org/10.1111/j.1751-908X.2005.tb00904.x

Kirchenbaur, M., Heuser, A., Bragagni, A., Wombacher, F. (2018) Determination of In and Sn Mass Fractions in Sixteen Geological Reference Materials by Isotope Dilution MC-ICP-MS. *Geostandards and Geoanalytical Research* 42, 361–377. https://doi.org/10.1111/ggr.12211

König, S., Münker, C., Hohl, S., Paulick, H., Barth, A.R., Lagos, M., Pfänder, J., Büchl, A. (2011) The Earth's tungsten budget during mantle melting and crust formation. *Geochimica et Cosmochimica Acta* 75, 2119–2136. https://doi.org/10.1016/j.gca.2011.01.031

Kumar, A., Bhaskar Rao, Y.J., Sivaraman, T.V., Gopalan, K. (1996) Sm-Nd ages of Archaean metavolcanics of the Dharwar craton, South India. *Precambrian Research* 80, 205–216. https://doi.org/10.1016/S0301-9268(96)00015-0

Kurzweil, F., Münker, C., Tusch, J., Schoenberg, R. (2018) Accurate stable tungsten isotope measurements of natural samples using a ^{180}W-^{183}W double-spike. *Chemical Geology* 476, 407–417. https://doi.org/10.1016/j.chemgeo.2017.11.037

Kurzweil, F., Münker, C., Hoffmann, J.E., Tusch, J., Schoenberg, R. (2020) Stable W isotope evidence for redistribution of homogeneous ^{182}W anomalies in SW Greenland. *Geochemical Perspectives Letters* 14, 53–57. https://doi.org/10.7185/geochemlet.2024

Leitzke, F.P., Pakulla, J.J., Tusch, J., Ravindran, A., Gordilho-Barbosa, R., Zincone, S.A., Hellers, M., Martins, A.A., Spreafico, R.R., Yang, R., Wombacher, F., Barbosa, J.S.F., Münker, C. (2024) Evidence for a missing late veneer from ^{182}W and ^{142}Nd systematics in the Archean São Francisco Craton. *Earth and Planetary Science Letters* 647, 119022. https://doi.org/10.1016/j.epsl.2024.119022

Liu, J., Pearson, D.G., Chacko, T., Luo, Y. (2018) A reconnaissance view of tungsten reservoirs in some crustal and mantle rocks: Implications for interpreting W isotopic compositions and crust-mantle W cycling. *Geochimica et Cosmochimica Acta* 223, 300–318. https://doi.org/10.1016/j.gca.2017.12.015

Maltese, A., Caro, G., Pandey, O.P., Upadhyay, D., Mezger, K. (2022) Direct evidence for crust-mantle differentiation in the late Hadean. *Communications Earth and Environment* 3, 12. https://doi.org/10.1038/s43247-022-00341-9

Maya, J.M., Bhutani, R., Balakrishnan, S., Rajee Sandhya, S. (2017) Petrogenesis of 3.15 Ga old Banasandra komatiites from the Dharwar craton, India: Implications for early mantle heterogeneity. *Geoscience Frontiers* 8, 467–481. https://doi.org/10.1016/j.gsf.2016.03.007

Mei, Q.-F., Yang, J.-H., Wang, Y.-F., Wang, H., Peng, P. (2020) Tungsten isotopic constraints on homogenization of the Archean silicate Earth: Implications for the transition of tectonic regimes. *Geochimica et Cosmochimica Acta* 278, 51–64. https://doi.org/10.1016/j.gca.2019.07.050

Messling, N., Jodder, J., Hegner, E., Hofmann, A., Wemmer, K., Willbold, M. (2023) Mobilization of Tungsten in Greenstone Belts of the Archean Kaapvaal and Singhbhum Cratons. *Geochemistry, Geophysics, Geosystems* 24, e2023GC011161. https://doi.org/10.1029/2023GC011161

Morino, P., Caro, G., Reisberg, L., Schumacher, A. (2017) Chemical stratification in the post-magma ocean Earth inferred from coupled ^{146,147}Sm–^{142,143}Nd systematics in ultramafic rocks of the Saglek block (3.25–3.9 Ga; northern Labrador, Canada). *Earth and Planetary Science Letters* 463, 136–150. https://doi.org/10.1016/j.epsl.2017.01.044

Münker, C., Wörner, G., Yogodzinski, G., Churikova, T. (2004) Behaviour of high field strength elements in subduction zones: constraints from Kamchatka–Aleutian arc lavas. *Earth and Planetary Science Letters* 224, 275–293. https://doi.org/10.1016/j.epsl.2004.05.030

Murphy, D., Rizo, H., O'Neil, J., Hepple, R., Wiemer, D., Kemp, A., Vervoort, J. (2021) Combined Sm-Nd, Lu-Hf, and ^{142}Nd study of Paleoarchean basalts from the East Pilbara Terrane, Western Australia. *Chemical Geology* 578, 120301. https://doi.org/10.1016/j.chemgeo.2021.120301

Nath, J.S., Ramakrishnan, M. (1981) *Early Precambrian supracrustals of southern Karnataka*. Geological Survey of India, Memoir 112, Calcutta.

O'Neil, J., Carlson, R.W., Francis, D., Stevenson, R.K. (2008) Neodymium-142 Evidence for Hadean Mafic Crust. *Science* 321, 1828–1831. https://doi.org/10.1126/science.1161925

O'Neil, J., Rizo, H., Boyet, M., Carlson, R.W., Rosing, M.T. (2016) Geochemistry and Nd isotopic characteristics of Earth's Hadean mantle and primitive crust. *Earth and Planetary Science Letters* 442, 194–205. https://doi.org/10.1016/j.epsl.2016.02.055

Pakulla, J.J., Jansen, M.W., Duraiswami, R.A., Gadpallu, P., Tusch, J., Jentzsch, C., Braukmüller, N., Wombacher, F., Münker, C. (2023) Trace element and Sr-Nd-Hf-Pb isotope evidence for a multi-magma chamber system beneath the Deccan Volcanic Province, India. *Chemical Geology* 640, 121749. https://doi.org/10.1016/j.chemgeo.2023.121749

Pakulla, J.J., Tusch, J., Hasenstab-Dübeler, E., Ravindran, A., Jansen, M.W., Leitzke, F.P., Gadpallu, P., Duraiswami, R.A., Münker, C. (2025) The spatio-temporal evolution of ^{182}W and ^{142}Nd in the Deccan-La Réunion plume. *Earth and Planetary Science Letters* 653, 119225. https://doi.org/10.1016/j.epsl.2025.119225

Puchtel, I.S., Blichert-Toft, J., Touboul, M., Horan, M.F., Walker, R.J. (2016a) The coupled ^{182}W-^{142}Nd record of early terrestrial mantle differentiation. *Geochemistry, Geophysics, Geosystems* 17, 2168–2193. https://doi.org/10.1002/2016GC006324

Puchtel, I.S., Touboul, M., Blichert-Toft, J., Walker, R.J., Brandon, A.D., Nicklas, R.W., Kulikov, V.S., Samsonov, A.V. (2016b) Lithophile and siderophile element systematics of Earth's mantle at the Archean–Proterozoic boundary: Evidence from 2.4 Ga komatiites. *Geochimica et Cosmochimica Acta* 180, 227–255. https://doi.org/10.1016/j.gca.2016.02.027

Ravindran, A., Mezger, K., Balakrishnan, S., Kooijman, E., Schmitt, M., Berndt, J. (2020) Initial ^{87}Sr/^{86}Sr as a sensitive tracer of Archaean crust-mantle evolution: Constraints from igneous and sedimentary rocks in the western Dharwar Craton, India. *Precambrian Research* 337, 105523. https://doi.org/10.1016/j.precamres.2019.105523

Ravindran, A., Mezger, K., Balakrishnan, S., Berndt, J. (2021) Hf-Nd isotopes from ultramafic and mafic rocks in the western Dharwar Craton, India, record early Archean mantle heterogeneity. *Lithos* 404–405, 106491. https://doi.org/10.1016/j.lithos.2021.106491

Ravindran, A., Mezger, K., Balakrishnan, S., Berndt, J., Ranjan, S., Upadhyay, D. (2023) Formation of Paleo- to Meso-Archean continental crust in the western Dharwar Craton, India: Constraints from U–Pb zircon ages and Hf-Pb-Sr isotopes of granitoids and sedimentary rocks. *Chemical Geology* 615, 121196. https://doi.org/10.1016/j.chemgeo.2022.121196

Ravindran, A., Peters, B.J., Mezger, K., Hasenstab-Dübeler, E., Maya, J.M., Schönbächler, M. (2024) Distinct Hadean Mantle Sources of Felsic and Mafic Terranes Juxtaposed in the Paleoarchean. *Geochemistry, Geophysics, Geosystems* 25, e2024GC011834. https://doi.org/10.1029/2024GC011834

Reimink, J.R., Chacko, T., Carlson, R.W., Shirey, S.B., Liu, J., Stern, R.A., Bauer, A.M., Pearson, D.G., Heaman, L.M. (2018) Petrogenesis and tectonics of the Acasta Gneiss Complex derived from integrated petrology and ^{142}Nd and ^{182}W extinct nuclide-geochemistry. *Earth and Planetary Science Letters* 494, 12–22. https://doi.org/10.1016/j.epsl.2018.04.047

Rizo, H., Boyet, M., Blichert-Toft, J., Rosing, M.T. (2013) Early mantle dynamics inferred from ^{142}Nd variations in Archean rocks from southwest Greenland. *Earth and Planetary Science Letters* 377–378, 324–335. https://doi.org/10.1016/j.epsl.2013.07.012

Rizo, H., Walker, R.J., Carlson, R.W., Touboul, M., Horan, M.F., Puchtel, I.S., Boyet, M., Rosing, M.T. (2016) Early Earth differentiation investigated through ^{142}Nd, ^{182}W, and highly siderophile element abundances in samples from Isua, Greenland. *Geochimica et Cosmochimica Acta* 175, 319–336. https://doi.org/10.1016/j.gca.2015.12.007

Saji, N.S., Larsen, K., Wielandt, D., Schiller, M., Costa, M.M., Whitehouse, M.J., Rosing, M.T., Bizzarro, M. (2018) Hadean geodynamics inferred from time-varying ^{142}Nd/^{144}Nd in the early Earth rock record. *Geochemical Perspectives Letters* 7, 43–48. https://doi.org/10.7185/geochemlet.1818

Sarma, D.S., Mcnaughton, N.J., Belusova, E., Mohan, M.R., Fletcher, I. R. (2012) Detrital zircon U–Pb ages and Hf-isotope systematics from the Gadag Greenstone Belt : Archean crustal growth in the western Dharwar Craton, India. *Gondwana Research* 22, 843–854. https://doi.org/10.1016/j.gr.2012.04.001

Srinivasaiah, C., Vasudev, V.N., Chalapathi Rao, N.V. (2015) Tungsten, Barium and Base Metal Mineralization in a Layer of Amphibolite in Mesoarchaean Ghattihosahalli Belt, Western Dharwar Craton, Karnataka, India. *Journal of the Geological Society of India* 86, 648–656. https://doi.org/10.1007/s12594-015-0356-7

Touboul, M., Puchtel, I.S., Walker, R.J. (2012) ^{182}W Evidence for Long-Term Preservation of Early Mantle Differentiation Products. *Science* 335, 1065–1069. https://doi.org/10.1126/science.1216351

Tusch, J., Sprung, P., van de Löcht, J., Hoffmann, J.E., Boyd, A.J., Rosing, M.T., Münker, C. (2019) Uniform ^{182}W isotope compositions in Eoarchean rocks from the Isua region, SW Greenland: The role of early silicate differentiation and missing late veneer. *Geochimica et Cosmochimica Acta* 257, 284–310. https://doi.org/10.1016/j.gca.2019.05.012

Tusch, J., Münker, C., Hasenstab, E., Jansen, M., Marien, C.S., Kurzweil, F., Van Kranendonk, M.J., Smithies, H., Maier, W., Garbe-Schönberg, D. (2021) Convective isolation of Hadean mantle reservoirs through Archean time. *Proceedings of the National Academy of Sciences* 118, e2012626118. https://doi.org/10.1073/pnas.2012626118

Tusch, J., Hoffmann, J.E., Hasenstab, E., Fischer-Gödde, M., Marien, C.S., Wilson, A.H., Münker, C. (2022) Long-term preservation of Hadean protocrust in Earth's mantle. *Proceedings of the National Academy of Sciences* 119, e2120241119. https://doi.org/10.1073/pnas.2120241119

Webb, P.C., Potts, P.J., Thompson, M., Gowing, C.J.B., Wilson, S.A. (2021) GeoPT49–An international proficiency test for analytical geochemistry laboratories – Report on Round 49 (Basalt, BVA-1) / July 2021. https://www.geoanalyst.org/wp-content/uploads/2023/03/GeoPT49-Full-Report.pdf

Yang, R., Gutjahr, M., Scholz, F., Kurzweil, F., Eroglu, S., Münker, C. (2025) Stable tungsten (W) isotope systematics in marine sediments: a potential paleo-proxy for deep ocean oxygenation. *Earth and Planetary Science Letters* 660, 119346. https://doi.org/10.1016/j.epsl.2025.119346